**RESEARCH ARTICLE** | *Sensory Processing*

# Functional characterization and spatial clustering of visual cortical neurons in the predatory grasshopper mouse *Onychomys arenicola*

**Benjamin Scholl,[1] Jagruti J. Pattadkal,[2] Ashlee Rowe,[3] and Nicholas J. Priebe[2]**

[1]*Functional Architecture and Development of Cerebral Cortex, Max Planck Florida Institute, Jupiter, Florida;* [2]*Department of Neuroscience, The University of Texas at Austin, Austin, Texas;* and [3]*Department of Integrative Biology and Neuroscience Program, Michigan State University, East Lansing, Michigan*

**Scholl B, Pattadkal JJ, Rowe A, Priebe NJ.** Functional characterization and spatial clustering of visual cortical neurons in the predatory grasshopper mouse *Onychomys arenicola*. *J Neurophysiol* 117: 910–918, 2017. First published December 7, 2016; doi:10.1152/jn.00779.2016.—Mammalian neocortical circuits are functionally organized such that the selectivity of individual neurons systematically shifts across the cortical surface, forming a continuous map. Maps of the sensory space exist in cortex, such as retinotopic maps in the visual system or tonotopic maps in the auditory system, but other functional response properties also may be similarly organized. For example, many carnivores and primates possess a map for orientation selectivity in primary visual cortex (V1), whereas mice, rabbits, and the gray squirrel lack orientation maps. In this report we show that a carnivorous rodent with predatory behaviors, the grasshopper mouse (*Onychomys arenicola*), lacks a canonical columnar organization of orientation preference in V1; however, neighboring neurons within 50 µm exhibit related tuning preference. Using a combination of two-photon microscopy and extracellular electrophysiology, we demonstrate that the functional organization of visual cortical neurons in the grasshopper mouse is largely the same as in the C57/BL6 laboratory mouse. We also find similarity in the selectivity for stimulus orientation, direction, and spatial frequency. Our results suggest that the properties of V1 neurons across rodent species are largely conserved.

**NEW & NOTEWORTHY** Carnivores and primates possess a map for orientation selectivity in primary visual cortex (V1), whereas rodents and lagomorphs lack this organization. We examine, for the first time, V1 of a wild carnivorous rodent with predatory behaviors, the grasshopper mouse (*Onychomys arenicola*). We demonstrate the cellular organization of V1 in the grasshopper mouse is largely the same as the C57/BL6 laboratory mouse, suggesting that V1 neuron properties across rodent species are largely conserved.

visual cortex; orientation selectivity; spatial frequency; cortical organization; functional organization; comparative physiology; carnivorous rodent

THE FUNCTIONAL ORGANIZATION of neocortical circuits has provided a scaffold for studying neural circuitry since it was first postulated anatomically and physiologically (de Nó 1949; Mountcastle 1957). Physiologically defined, neurons sharing particular response properties and overlapping sensory recep-tive field locations are arranged in columns across the cortical surface. How this circuit organization emerges and its greater importance for processing remain elusive, despite its pervasive appearance across cortical areas in mammals (Horton and Adams 2005). Columnar organization of orientation selectivity in primary visual cortex (V1), first demonstrated in carnivores (Bonhoeffer and Grinvald 1991; Hubel and Wiesel 1962, 1963) and then in primates (Essen and Zeki 1978; Hubel and Wiesel 1968; Ts'o et al. 1990), is a prime example of this emergent functional architecture. A smooth organization of orientation selectivity in V1 also exists for ferrets (Chapman et al. 1996; Nauhaus et al. 2012b), Etruscan tree shrews (Bosking et al. 1997; Weliky et al. 1996), and New World primates (McLoughlin and Schiessl 2006; O'Keefe et al. 1998; Xu et al. 2004). Rodents, however, do not possess an orientation map and instead exhibit a random or "salt-and-pepper" organization (Ohki et al. 2005; Ohki and Reid 2007; Van Hooser et al. 2005). Despite a salt-and-pepper organization in mouse, recent studies report small, short-distance correlations between neighboring neuron response properties (Ringach et al. 2016).

The factors determining whether a columnar architecture emerges in visual cortex remain opaque. Whereas body and brain size are weakly correlated with the emergence of orientation columns (Keil et al. 2012; Van Hooser et al. 2005), there are a number of outliers such as small animals possessing columns (pigmy marmosets; McLoughlin and Schiessl 2006) and larger ones that do not (lagomorphs; Murphy and Berman 1979). Peripheral acuity might play a role since mammals with a cone-based visual system are weakly linked to a columnar organization (Keil et al. 2012; Van Hooser et al. 2005; Van Hooser 2007), but again, outliers such as the nocturnal owl monkey and prosimian bushbaby with little or no retinal foveal cone specialization (Ogden 1975; Wikler and Rakic 1990) still possess an orientation map in V1 (O'Keefe et al. 1998; Xu et al. 2004, 2005).

Another potential factor is the relationship between species behavior and columnar architecture. Mammals exhibiting predatory behaviors (carnivores and primates) often posses orientation columns, whereas scavengers and potential prey for larger creatures (rodents and lagomorphs) lack functional organization (Keil et al. 2012; Van Hooser et al. 2005; Van Hooser 2007). Predatory or carnivorous behaviors may provide a constraint that imposes a columnar organization for orienta-

Address for reprint requests and other correspondence: N. J. Priebe, Dept. of Neuroscience, The Univ. of Texas at Austin, 2400 Speedway, Austin, TX 78712 (e-mail: nicholas@mail.utexas.edu).

tion selectivity. In this article we address whether a carnivorous rodent, the grasshopper mouse (*Onychomys arenicola*), has a columnar organization of orientation selectivity in V1. Unlike other rodents that are strictly herbivorous or that facultatively consume insects, grasshopper mice are obligate carnivores (Horner et al. 1964; Landry 1970), preying on a wide range of invertebrate and vertebrate species, including other mammals (Horner et al. 1964; Ruffer 1968; Timberlake and Washburne 1989). Grasshopper mice are aggressive hunters and tenacious predators that have developed resistance to many aversive tactics by their prey (Langley 1994; Rowe and Rowe 2008; Rowe et al. 2013; Timberlake and Washburne 1989). Whereas most animals learn to avoid noxious prey, grasshopper mice persistently attack arthropods (insects, scorpions, spiders, and centipedes) with formidable defenses, enabling them to exploit prey avoided by other species (Rowe et al. 2013; Sarko et al. 2011).

Using extracellular single-unit recordings and two-photon calcium imaging, we find that the grasshopper mouse cortical organization is similar to that of the inbred C57/BL6 laboratory mouse. Calcium imaging revealed a random salt-and-pepper map of orientation preference in both rodent species, evidence against a canonical columnar organization. Both species did, however, exhibit orientation preference similarity between nearby neighboring neurons, and this spatially dependent relationship was more pronounced in the grasshopper mice. Across populations, tuning strength and orientation preferences also were similar between animals. Spatial frequency sensitivity in individual neurons also was similar between animals. These results are not consistent with the prediction that functional columnar organization in V1 is determined by predatory vs. scavenger behaviors, and instead suggest that other factors drive the emergence of functional columns.

## METHODS

All procedures were approved by The University of Texas at Austin Institutional Animal Care and Use Committee.

*Physiology.* Physiological procedures for mouse recordings were based on those previously described (Scholl et al. 2013a). Experiments were conducted using adult C57BL/6 mice ($n = 10$, age 5–8 wk) and *O. arenicola* grasshopper mice ($n = 11$, age 8–24 mo). In combination with 1,000 mg/kg urethane and 10 mg/kg chlorprothixene, isoflurane (0.25–2.0%) was administered during surgery and the experiment duration to eliminate a pedal withdrawal reflex. Brain edema was prevented using 20 mg/kg dexamethasone. Animals were warmed with a thermostatically controlled heat lamp to maintain body temperature at 37°C. A tracheotomy was performed. The head was placed in a mouse adaptor (Stoelting), and a craniotomy and duratomy were preformed over visual cortex. Mice eyes were kept moist with a thin layer of silicone oil. The contralateral eye was stimulated during the recording. Primary visual cortex was located and mapped by multiunit extracellular recordings with tungsten electrodes (1 MΩ; Micro Probes). The V1/V2 boundary was identified by the characteristic gradient in receptive locations (Dräger 1975; Métin et al. 1988). Eye drift under urethane anesthesia is typically small and results in a change in eye position of <2° per hour (Sarnaik et al. 2014).

*Extracellular recordings.* Extracellular electrodes (1 MΩ; Micro Probes) were advanced into cortex with a motorized drive (MP-285; Sutter Instrument). After the electrode was in place, warm agarose solution (2–4% in normal saline) was placed over the craniotomy to protect the surface of the cortex and reduce pulsa-

tions. Action potentials were identified using a dual time and amplitude window discriminator (DDIS-1; Bak Electronics). The time of action potentials and raw extracellular traces were recorded for later analysis.

*Dye loading and in vivo two-photon microscopy.* Bulk loading of a calcium-sensitive dye under continuous visual guidance followed previous protocols (Garaschuk et al. 2006; Golshani and Portera-Cailliau 2008; Grienberger and Konnerth 2012; Kerr et al. 2005; Stosiek et al. 2003). The cortical visuotopic region targeted for loading was mapped with extracellular methods prior to loading. Dye solution contained 0.8 mM Oregon green 488 BAPTA-1 AM (OGB-1 AM; Invitrogen) dissolved in DMSO (Sigma-Aldrich) with 20% Pluronic acid (Sigma-Aldrich) and mixed in a salt solution (150 mM NaCl, 2.5 mM KCl, and 10 mM HEPES, pH 7.4; all Sigma-Aldrich). Either 40–80 $\mu$M Alexa Fluor 594 (Invitrogen) or 125 $\mu$M Sulforhodamine 101 (Sigma-Aldrich) was also included. A patch pipette (tip diameter 2–5 $\mu$m; King Precision Glass) with this solution was inserted into the cortex to a depth of 250–400 $\mu$m below the surface. The solution was carefully pressure injected (100–350 mbar) over 10–15 min. After 1 h, the cortex was sealed with 1.5% agarose (in saline), a glass coverslip, and metal springs to apply pressure and reduce brain pulsations. Fluctuations in calcium fluorescence were collected with a custom-built two-photon microscope and a mode-locked Chameleon Ultra Ti:Sapphire laser (Coherent). Excitation light was focused by a ×40 objective (0.8 numerical aperture, Nikon; or 1.0 numerical aperture, Zeiss). Images were obtained with custom software (LabVIEW; National Instruments). Two different scanning mirror systems were used to collect data: a galvanometer system scanning at 4-Hz frame rate ($n = 4$ *O. arenicola* mice; $n = 3$ C57/BL6 mice) and a resonant mirror system scanning at 30-Hz frame rate ($n = 7$ *O. arenicola* mice; $n = 2$ C57/BL6 mice). With the galvanometer system, square regions of cortex 150 $\mu$m wide were imaged at 150 × 150 pixels. With the resonant mirror system, a square region of cortex 300 $\mu$m wide was imaged at 256 × 455 pixels. Images in all experiments were obtained from at least three depths separated by 20–25 $\mu$m, starting at least 150 $\mu$m below the cortical surface.

*Stimuli.* Visual stimuli were generated by a Macintosh computer (Apple) using the Psychophysics Toolbox (Brainard 1997; Pelli 1997) for MATLAB (The MathWorks) and presented using a SONY video monitor (GDM-F520) placed 25 cm from the animal's eye. The video monitor had a noninterlaced refresh rate of 100 Hz and a spatial resolution of 1,024 × 768 pixels, which subtended 40 × 30 cm. The video monitors had a mean luminance of 40 cd/cm². Drifting gratings (40° diameter, 0.02–0.04 spatial frequency, 100% contrast, 2- to 4-Hz temporal frequency) were presented for 2–3 s in both electrophysiology and imaging experiments. Stimuli were preceded and followed by 250-ms or 2- to 3-s blank (mean luminance) periods for physiology and imaging, respectively. Spontaneous activity was measured during blank (mean luminance) periods pseudorandomly interleaved with drifting grating stimuli. During imaging sessions, the stimulation protocol was repeated seven to eight times at each focal plane. The microscope objective and photomultipliers were shielded from stray light and the video monitors.

*Electrophysiology analysis.* Spiking responses for each stimulus were cycle-averaged across trials following removal of the first cycle. The Fourier transform was used to calculate the mean ($F_0$) and modulation amplitude ($F_1$) of each cycle-averaged response, and afterward, mean spontaneous activity was subtracted. Peak responses were defined as the sum of the mean and modulation ($F_0 + F_1$). A double Gaussian curve was fit to responses for characterizing orientation/direction preference (Carandini and Ferster 2000):

$$R(\theta) = \alpha e^{-(\theta - \theta_{pref})/(2\sigma^2)} + \beta e^{-(\theta - \theta_{pref} + \pi)/(2\sigma^2)} + spont,$$

where $R(\theta)$ is the response of the neuron to different orientations $\theta$, $\sigma$ is the width of the tuning curve, *spont* is the mean spontaneous activity, $\alpha$ and $\beta$ are peak amplitudes, and $\theta_{pref}$ is the orientation

preference. The orientation selectivity index was also computed (Ringach et al. 2002; Tan et al. 2011):

$$OSI = \frac{\sqrt{\left[\sum R(\theta)\sin(2\theta)\right]^2 + \left[\sum R(\theta)\cos(2\theta)\right]^2}}{\sum R(\theta)},$$

where $R(\theta)$ is the response of the neuron to different orientations $\theta$. Direction selectivity was computed as follows:

$$DSI = \frac{R_{pref} - R_{null}}{R_{pref} + R_{null}},$$

where $R_{pref}$ is the response to the preferred stimulus and $R_{null}$ is the response the stimulus in the opposite direction.

*Imaging analysis.* Images were analyzed with custom MATLAB software (The MathWorks). Cells were identified by hand from structure images on the basis of size, shape, and brightness. Cell masks were generated automatically (Nauhaus et al. 2012a; Scholl et al. 2015). Individual neuron time courses were extracted by summing pixel intensity values within cell masks in each frame. If brain pulsations were evident in time courses, these data were not used. Responses ($F_t$) to each stimulus presentation were normalized by the response to the gray screen ($F_o$) immediately before the stimulus came on:

$$\Delta F/F = (F_t - F_o)/F_o.$$

For each stimulus, the mean change in fluorescence ($\Delta F/F$) was calculated in a 0.5-s window, centered around the global average peak calculated by averaging responses to all stimulus conditions and trials. Visually responsive cells were defined by having at least one response significantly larger than spontaneous activity (ANOVA, $P < 0.05$). Stimulus preferences characterized using the same equations shown above.

*Correlation computation.* Tuning correlation between two neurons was computed as the Pearson correlation coefficient between the baseline subtracted peak responses across all different grating responses for both neurons.

## RESULTS

*Characterization of orientation selectivity and spatial frequency.* We compared the functional architecture of primary visual cortex (V1) of the C57/BL6 laboratory mouse with that of the carnivorous grasshopper mouse *O. arenicola* (Fig. 1*A*). We first identified the location of V1 (Fig. 1*B*), following the anatomical pattern suggested by cyctochrome oxidase staining (Sarko et al. 2011), and performed extracellular recordings from single units both to establish the basic retinotopic organization and determine whether orientation selectivity was a property of these neurons.

A broad spectrum of orientation selectivity is observed in both C57/Bl6 mice as well as grasshopper mice: some neurons are exquisitely selective for orientation (Fig. 1*A*, *middle*) whereas others were unselective for stimulus orientation (Fig. 1*A*, *bottom*). Each cell's selectivity or lack thereof was characterized by an orientation selectivity index (OSI; see METHODS). An OSI of 1 indicates a neuron responds to a single orientation, whereas an OSI of 0 indicates equal responses across orientations (Ringach et al. 2002; Tan et al. 2011). A comparison between cell populations from C57/Bl6 and grasshopper mice showed the extent of selectivity in V1 was comparable (Fig. 1*B*), but neurons recorded in the grasshopper mice were slightly less selective for oriented gratings [*O. arenicola*: median OSI = 0.24, mean OSI = 0.27 ± 0.22 (SD), $n = 41$; C57/BL6: median OSI = 0.33, mean OSI = 0.33 ± 0.14 SD, $n = 45$; $P = 0.001$, Mann-Whitney test; Fig. 1*C*].

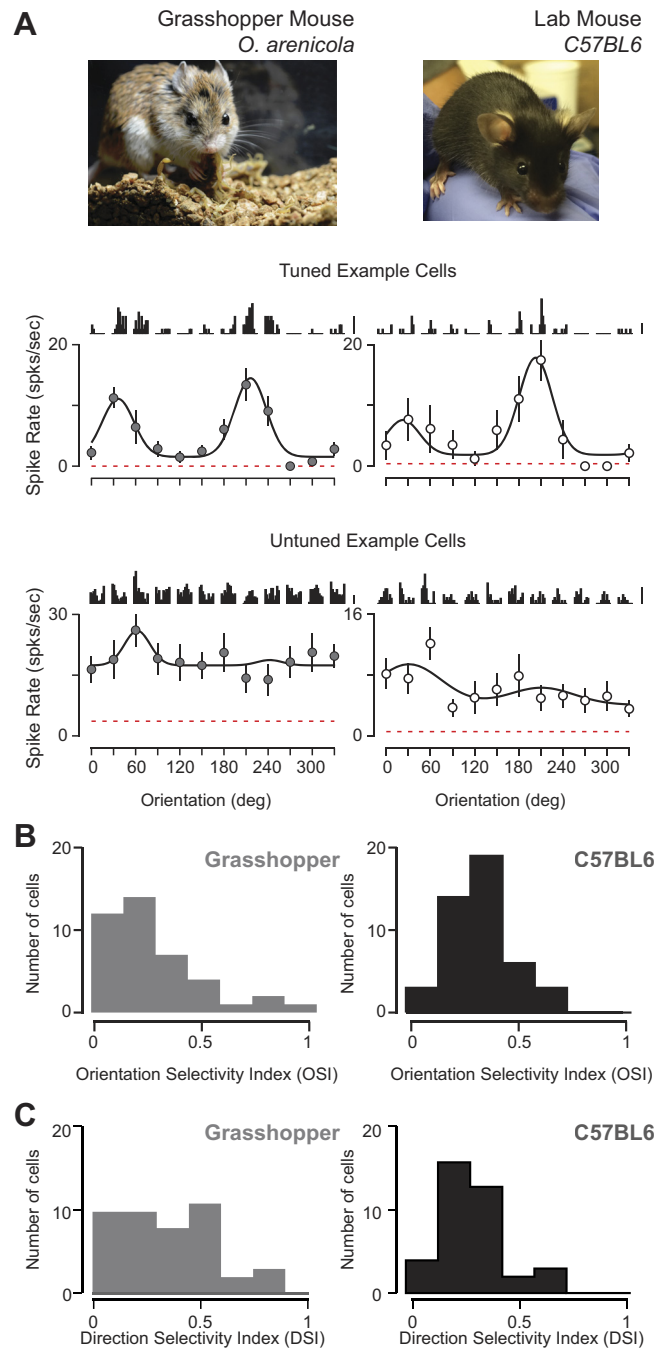

Fig. 1. Orientation selectivity in primary visual cortex of predatory grasshopper and laboratory mice. *A*: carnivorous grasshopper mouse (*Onychomys arenicola*; *top left*; picture courtesy of A. H. Rowe) and C57/BL6 laboratory mouse (*top right*). Example orientation tuning curves of spiking responses from neurons in V1 (*middle* and *bottom*) shown mean cycle-averaged responses to each presentation of each oriented grating above the peak ($F_0 + F_1$) spiking responses. Time course of cycle-averaged responses is 250 ms. Scale bars are 10 spikes/s. Dashed red line indicates spontaneous firing rate. Curve fits are a double Gaussian (see METHODS). *B*: distributions of orientation selectivity index (OSI) in both rodents. *C*: distributions of direction selectivity index (DSI) in both rodents.

From these data we also computed a direction selectivity index (DSI; see METHODS) and found slightly higher DSI for grasshopper mice (*O. arenicola*: median DSI = 0.31, mean DSI = 0.39 ± 0.29; C57/BL6: median DSI = 0.29, mean DSI = 0.35 ± 0.26; $P = 0.01$, Mann-Whitney test; Fig. 1*C*).
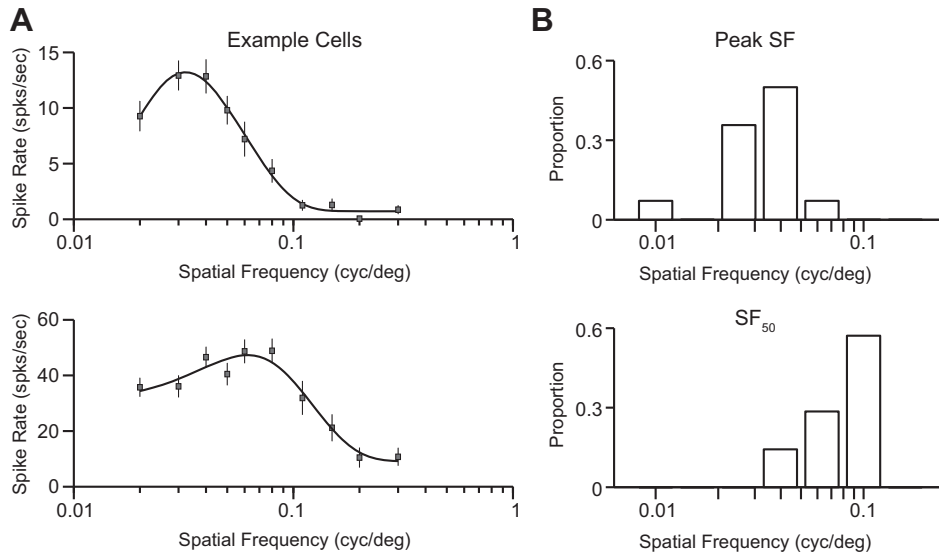
**A**



**B**



Fig. 2. Spatial frequency sensitivity in predatory grasshopper mice. (*A*) Example tuning curves of spiking responses from two V1 neurons. Drifting gratings with optimal orientation, direction, and spatial location for each neuron were shown at varying spatial frequencies. Shown are mean cycle-averaged responses to each presentation of each oriented grating above the peak ($F_o$ + $F_1$) spiking responses. Curve fits are a Difference of Gaussians. (*B*) Distributions of the spatial frequency eliciting the largest responses (Peak, *top*) and the highest spatial frequency eliciting a spiking response 50% of the maximum responses ($SF_{50}$, *bottom*).

Spatial frequency sensitivity was measured during extracellular recordings from grasshopper mice by using drifting gratings of the optimal orientation, direction, and receptive field location. Across our population we found a modest diversity of tuning preferences and sensitivity range, with both low-pass (Fig. 2*A*, *top*) and bandpass (Fig. 2*A*, *bottom*) tuning observed in individual neurons. Overall, spatial frequencies eliciting the strongest spiking responses were low compared with those in other carnivores (median = 0.036, mean = 0.035 ± 0.01, $n$ = 14; Fig. 2*B*, *top*) and matched those reported by Neill and Stryker (2008) in the C57/BL6 laboratory mouse. The highest spatial frequencies to evoke responses 50% of the maximum response ($SF_{50}$) were also low compared with those in other carnivores (median = 0.09, mean = 0.083 ± 0.03, $n$ = 14; Fig. 2*B*, *bottom*).

Because we typically record from multiple neurons within a single electrode penetration, we were able to assess whether there is a columnar organization of orientation preference similar to that in other carnivores and primates (Hubel and Wiesel 1963). In tangential penetrations of V1 in grasshopper mice, we recorded from several single units, evident from distinct isolated waveforms (Fig. 3*A*; see METHODS). After passing the electrode through the cortical tissue, we injected current (2 nA, 1–2 s) to lesion for histology. We performed a Nissl stain to recover the lesion and electrode tract (Fig. 3*A*, *left inset*), from which we were able to reconstruct our tangential penetration (Hubel and Wiesel 1963). Even within a single penetration, we observed a wide range of orientation preferences, depicted in this example by elongated bars and the

actual computed preference from Gaussian fits of spiking responses (Fig. 3*A*). For each tangential penetration with at least two selective cells (OSI > 0.10), we computed the distance between cells and the absolute value of their orientation preference difference (Fig. 3*B*). We found no relationship between cell distance and preference dissimilarity from extracellular recordings in the grasshopper mouse [*O. arenicola*: $r$ = 0.18, $P$ = 0.66, circular-linear correlation coefficient (Batschelet 1981)].

*Cellular cortical organization of orientation preference and tuning correlation.* Although we found no evidence for a columnar organization of orientation preference in grasshopper mice, our extracellular measurements sampled coarsely over cortical space (mean pair distance = 236 ± 181 μm) may preclude the identification of fine-scale organization or spatial clusters. We therefore performed in vivo two-photon calcium imaging of bulk-loaded OGB-1 to quantify the degree of organization at the cellular level (see METHODS) (Garaschuk et al. 2006; Golshani and Portera-Cailliau 2008; Grienberger and Konnerth 2012; Kerr et al. 2005; Scholl et al. 2015; Stosiek et al. 2003). After receptive field locations were mapped from V1 with extracellular multiunit activity, hundreds of neurons were loaded with a calcium indicator in a 200- to 300-μm area (Fig. 4, *A* and *B*, *left*). Changes in calcium fluorescence (ΔF/F) from labeled neurons were measured in response to oriented drifting gratings (0°–315°) at multiple depths separated by 20–25 μm. Time courses of activity were generated for each cell by averaging pixels within each cell's mask across all imaging frames (Fig. 4, *A* and *B*, *left*; see METHODS). Our visual response
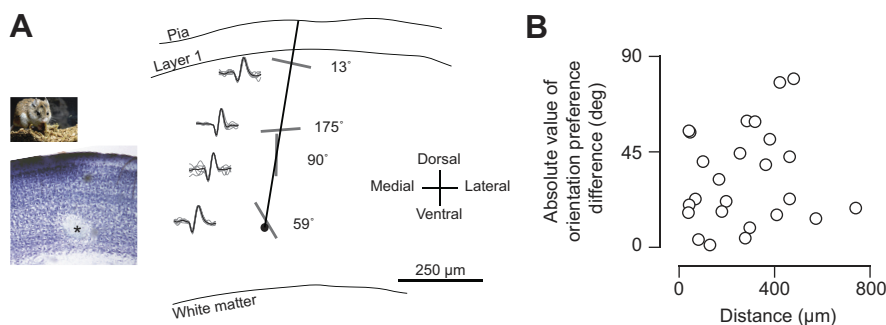
**A**



**B**



Fig. 3. Orientation preferences along tangential electrode recording tract in grasshopper mice. (*A*) Example extracellular recordings along reconstructed along tangential recording tract. Nissl stain of fixed brain slice with microelectrode current lesion (asterisk) shown in inset. Separate single unit recordings shown along tract with example action potential waveforms and oriented bars depicting orientation preferences. (*B*) Relationship of absolute value of orientation preference difference and distance between recordings within single penetrations.
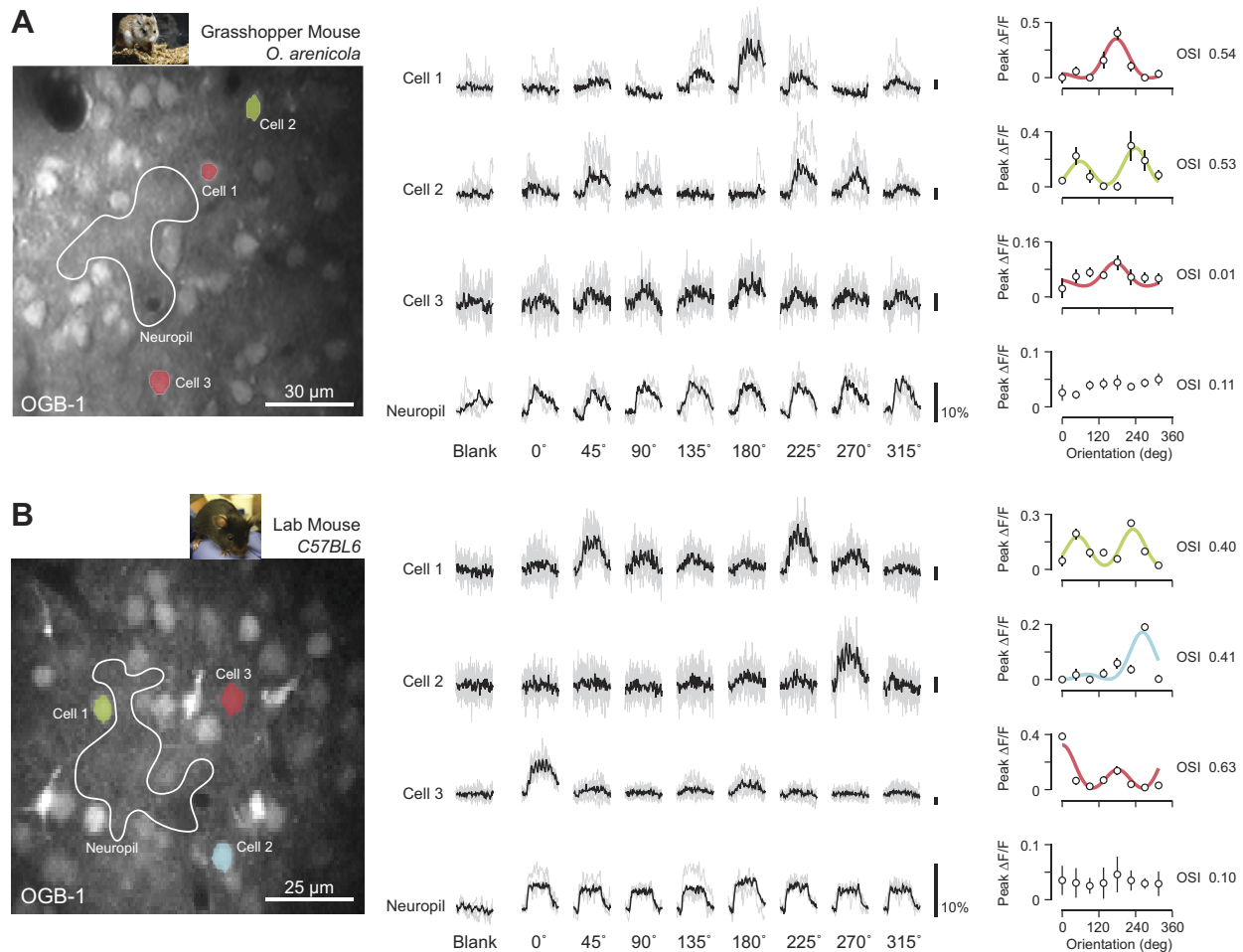
Fig. 4. Two-photon calcium imaging of predatory grasshopper and lab mice. (A) Example structural image of OGB-1 fluorescence collected from a grasshopper mouse (*left*). Three example V1 cell masks overlaid and color-coded based on preferences. Example neuropil mask also shown (white outline). Scale bar is 30 microns. Individual trial and mean changes in fluorescence (ΔF/F) to each visual stimulus and blank (mean luminance) periods shown for each example cell and neuropil (*middle*). Time course of responses is 2 sec and scale bars are 10% ΔF/F. Mean ΔF/F across stimuli plotted for each cell (*right*). Data fit with double Gaussian and color-coded based for orientation preference. (B) Same as in (a) for example imaging session in a lab mouse.

criterion required cells to have a significant response to at least one grating, relative to the blank luminance period (ANOVA, $P < 0.05$; see METHODS). Across all C57/BL6 laboratory mice ($n = 4$, age 1–2 mo) we identified a total of 1,814 neurons, of which 1,117 were visually responsive (62%). Across all grasshopper mice ($n = 7$, age 8–24 mo) we identified 2,199 neurons, of which 930 were visually responsive (42%).

Oriented gratings drive clear changes in calcium florescence in grasshopper mice (Fig. 4A) and C57/BL6 laboratory mice (Fig. 4B), relative to the fluorescence observed before stimulation or in response to a gray screen. Some neurons are highly selective for orientation, as indicated by the narrow range of orientations evoking fluorescence changes (Fig. 4A, *cell 1*). Trial-averaged mean responses were used to construct tuning curves, which were fit with a double Gaussian (Carandini and Ferster 2000) (Fig. 4A, *right*; see METHODS). As with our extracellular records, we quantified the degree of orientation selectivity using the OSI and direction selectivity using the DSI. The example neuron (*cell 1*) was very selective for both orientation (OSI = 0.54) and direction (DSI = 1.0). Across our sample populations we found neurons that were equally selective but showed varying degrees of direction selectivity (Fig. 4A, *cell 2*). Other

neurons exhibited little selectivity, despite being activated by the visual stimulus (Fig. 4A, *cell 3*). Individual neurons were distinct from the weakly active and untuned background neuropil change in florescence (Fig. 4A, neuropil), which is a criterion for inclusion in our data set (see METHODS). Similar degrees of orientation selectivity were observed when responses of individual V1 neurons in C57/BL6 laboratory mice were examined (Fig. 4B).

Overall, our optical measurements agreed with the electrophysiological comparison between animals. Neurons from grasshopper mice were slightly less tuned, but both rodent species exhibited the same extent of selectivity (grasshopper mouse: median OSI = 0.19, mean OSI = 0.24 ± 0.17, $n = 930$; laboratory mouse: median OSI = 0.25, mean OSI = 0.31 ± 0.21, $n = 1,114$; $P < 0.01$, Mann-Whitney test; Fig. 5, *A* and *B*). Distributions of DSI were similar in both animals (grasshopper mouse: median DSI = 0.32, mean DSI = 0.39 ± 0.28, $n = 930$; laboratory mouse: median DSI = 0.29, mean DSI = 0.35 ± 0.26, $n = 1,114$). We also found similar biases in distributions of orientation preference between animals for cells with at least modest OSI (>0.10). Specifically, both grasshopper and laboratory mice displayed some cardinal bias (Fig. 5, *C* and *D*).
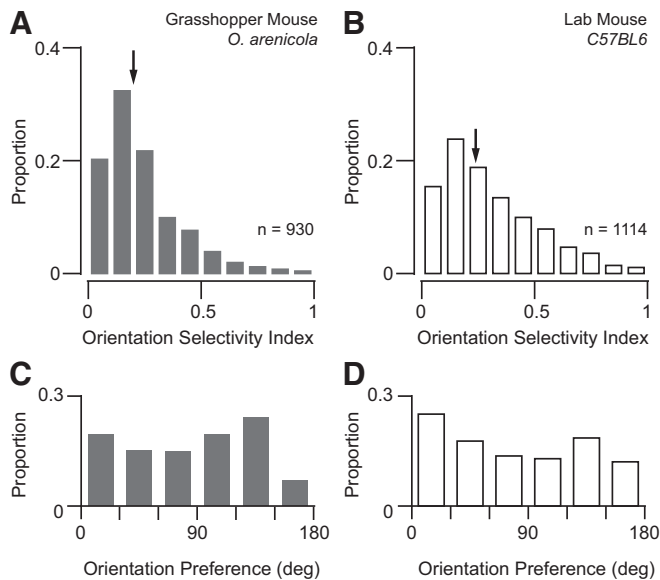
Fig. 5. Distributions of orientation selectivity and preference from two-photon imaging. (*A–B*) Distributions of orientation selectivity index (OSI) from calcium responses for grasshopper and lab mice (respectively). Arrows indicate median values for each population. (*C–D*) Distributions of orientation preference from neurons with an OSI at least greater than 0.15 for grasshopper and lab mice (respectively).

Large-scale maps of direction (0°–315°) and orientation (0°–135°) preferences in individual neurons showed that both the predatory grasshopper mouse and C57/BL6 lab mouse lack the strong functional organization in layer 2/3 of V1 found in primates and carnivores (Nauhaus et al. 2012b; Ohki et al. 2005) (Fig. 6). This organization has previously been characterized as random, or "salt-and-pepper" (Ohki and Reid 2007). In an example imaging session from a grasshopper mouse (Fig. 6*A*), cellular masks were color-coded on the basis of their
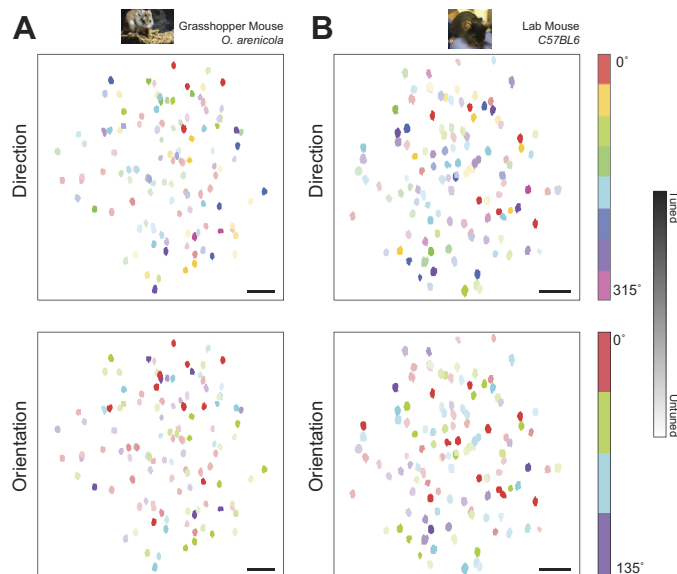
preference for a particular direction (*top*) or orientation (*bottom*), with the color intensity modulated according to each cell's OSI. For this illustration, cellular locations were also collapsed across multiple focal planes (190–270 $\mu$m below the pia). Both the map of directional preferences and the map of orientation preference lacked a global, columnar organization in the grasshopper mouse (Fig. 6*A*), as found in the C57/BL6 laboratory mouse (Fig. 6*B*) and in agreement with our tangential electrode penetrations (Fig. 3*B*).

Recently, fine-scale functional organization has been demonstrated in the C57/BL6 laboratory mouse in the form of spatial clustering: weak correlation of receptive field properties between nearby neighboring neurons (Ringach et al. 2016). To compare spatial clustering in the grasshopper and laboratory mouse, we computed the cortical distance and tuning correlation between neighboring neurons with at least moderate selectivity (OSI > 0.10; grasshopper mouse: $n = 582$, laboratory mouse: $n = 825$) using the full range of grating responses (0°–315°). Cortical distance was calculated using each neuron's *x-y* within-plane location and depth from the pia. Across all animals and neurons imaged we found that nearby neighboring neurons share similar tuning (<50 $\mu$m) in both rodent species (Fig. 7). Interestingly, we found that V1 neurons in the grasshopper mouse showed much larger correlation at short cortical distances (Fig. 7). However, an exponential fit to these data showed that the spatial length constants ($\lambda$; Scholl et al. 2015) were almost identical (grasshopper mouse: $\lambda = 33.6$ $\mu$m; laboratory mouse: $\lambda = 33.0$ $\mu$m). We also computed distance-dependent correlations while excluding neurons in focal planes directly above or below (*z* distance > 40 $\mu$m) and found no difference in the spatial trend. The similarity in response properties and organization between these two species suggests a common architecture for V1 in order Rodentia.

## DISCUSSION

We compared the functional architecture of V1 in C57/BL6 mice with that of a predatory rodent, the grasshopper mouse (*O. arenicola*), by using extracellular single-unit recordings and two-photon calcium imaging. Neurons in both rodent species exhibited similar degrees of orientation selectivity,
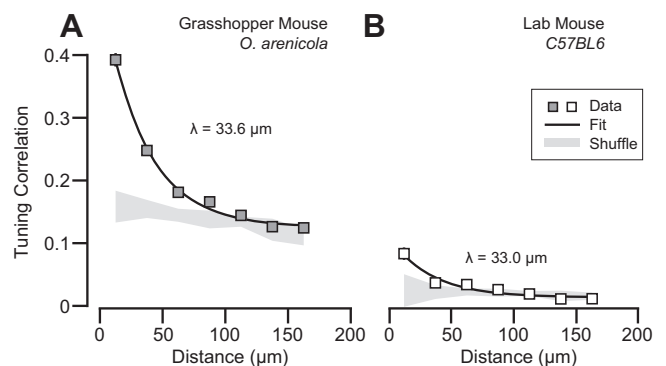


Fig. 6. Random 'salt-and-pepper' micro-organization of direction and orientation preference in grasshopper and lab mice. (*A*) Example map of direction (*top*) and orientation (*bottom*) preferences in V1 neurons of a grasshopper mouse. Color intensity indicates individual cell orientation selectivity index (OSI). Map generated by collapsing across depth (190–270 microns). Scale bar is 50 microns. (*B*) Same as in (a) for imaging session in a lab mouse (depths 275–340 microns).



Fig. 7. Tunining similarity depends on cortical distance in grasshopper and lab mice. (*A*) Relationship of cortical distance between neighboring cells and the correlation of their responses to the full set of gratings presented (0–315 deg) for grasshopper mice. Shown are the mean correlation and standard error for each group (boxes, gray fill). An exponential fit (black line) is plotted alongside the data. Gray shading is the mean correlation and 95% confidence interval from populations with shuffled neuron xyz positions. (*B*) Same as (a) for data from lab mice.

direction selectivity, and spatial frequency sensitivity, measured by both extracellular recordings and calcium imaging. However, cells in the grasshopper mouse tend to be slightly less selective. Two-photon imaging revealed a random "salt-and-pepper" map of orientation preference in both animals. Although we found no evidence for orientation columns in the grasshopper mouse, we did observe spatial clusters in the form of short-range ($<50$ $\mu$m) similarity in tuning as reported in the laboratory mouse (Ringach et al. 2016). Furthermore, spatial dependence of tuning similarity was almost identical between both animals ($\lambda \sim 30$–$33$ $\mu$m) and near that reported in the laboratory mouse ($\lambda = 38$ $\mu$m; Ringach et al. 2016). The similarity between our laboratory mouse correlation measurements with those of Ringach et al. (2016) is encouraging, given that their stimulus set was more diverse, they recorded from awake animals, and they processed the calcium responses using a different set of tools to compute correlations. By comparing the functional architecture within the order Rodentia, we demonstrate that the absence of a functional architecture in V1 is not due to either the selective pressure imposed by human domestication or the lack of predatory behavior in many rodents.

Over a century ago, C.C. Little and colleagues generated the C57/BL6 mouse at Cold Spring Harbor Laboratory, thereby creating what is now the most commonly studied mammal. This mouse strain required massive selective pressure by humans: repeated inbreeding of brothers and sisters to generate homozygous animals. As a consequence of this artificial selection, these animals are highly domesticated, having potentially lost the senses necessary for locating food and water as they would in natural environments. When we observe a distinct phenotype in C57/BL6 mice, we must therefore wonder whether that phenotype reflects the artificial selection process imposed or a preserved characteristic of these animals in their natural condition. We suspected that the response properties and functional architecture of neocortical neurons might be particularly sensitive to inbreeding, because the neocortex is the most recently developed neural structure in the mammalian brain (DeFelipe 2011; Rakic 2009). However, our records suggest that the lack of a functional organization for orientation preference in C57/BL6 mice, relative to carnivores and primates, is not due to selective breeding.

We naively hypothesized that predatory behavior might drive the emergence of orientation columns, since predatory species, such as primates and carnivorans, exhibit orientation columns whereas prey species, such as lagomorphs and rodents, lack this organization. The lack of orientation columns in predatory rodents suggests the absence of columns is a common phenotype of lagomorpha and rodentia, independent from how these mammals locate resources. In fact, limited evidence from newborn lambs suggests that even herbivores outside the Lagomorpha and Rodentia orders possess a columnar organization of orientation preference in V1 (Ramachandran et al. 1977). It is interesting that this functional divergence exists between different mammalian species, since rodents are more closely related to primates than cats. The presence of a common phenotype in distantly related mammals indicates that either orientation columns originated from a common mammalian ancestor and this phenotype was lost in rodents and lagomorphs, or that environmental pressure led to convergent evolution of orientation columns in primates and carnivorans.

Given the effort to understand the emergence of this organization in neocortical circuits, it is surprising that a restricted subset of mammals have been examined, mainly rodents, lagomorphs, primates, and carnivorans.

Differences in the sensory apparatus may be a determining factor for V1 functional organization. In carnivores and primates, the retinas exhibit central zones of high photoreceptor density, a region denoted as either an area centralis or fovea (Van Hooser et al. 2005; Van Hooser 2007). These spatially restricted zones of high retinal sampling are absent in mice (Jeon et al. 1998), although rabbits have a high-density streak in the distribution of retinal ganglion cells (Hughes 1971), as do carnivorous grasshopper mice (Clark et al. 2014). Areas of high photoreceptor and ganglion cell density impose physical constraints on the transformation of visual signals in retinas, since many neurons must be packed into a small territory. Because C57/BL6 mice have a relatively uniform density of ganglion cells, there may be little physical constraint and retinal ganglion cells may exhibit distinct functional properties. In fact, at least 30 distinct types of retinal ganglion cells have been identified in the C57/BL6 mouse, some of which are selective for specific features of visual stimuli (Sanes and Masland 2015). In contrast, both cat and primate retinae are dominated by fewer retinal ganglion cell classes (Dacey 1994). In particular, retinas from cat and primate are dominated by a single ganglion cell type, the midget ganglion cell, which is either absent or only weakly present in the mouse retina (Sanes and Masland 2015). Orientation bias is present in a fraction of retinal ganglion cells in cats and primates (Cleland and Levick 1974; Levick and Thibos 1982; Passaglia et al. 2002), and orientation/direction selectivity has been observed in thalamic relay cells of cats and primates (Cheong et al. 2013; Daniels et al. 1977; Lee et al. 1979; Soodak et al. 1987; Vidyasagar and Urbas 1982; Xu et al. 2002). However, the extent is far weaker compared with that in rodents (Marshel et al. 2012; Piscopo et al. 2013; Scholl et al. 2013b; Zhao et al. 2013). The progression of orientation selectivity in the early visual pathway of gray squirrels is similar to that of rodents and cats, despite their lack of orientation columns in visual cortex (Van Hooser et al. 2005; Zaltsman et al. 2015). The presence of orientation selective neurons in the sensory periphery may also be critical for determining visual cortex organization (Zhao et al. 2013). Likewise, the circuitry necessary to compute orientation and direction selectivity centrally in carnivorans and primates may impose constraints on or be inherently linked to the functional organization absent in rodents.

Although we do not understand the conditions necessary for functional architecture to emerge, cortical columns have been an important scaffold in dissecting the development and operation of neocortical circuits (Kaschube et al. 2010). We have shown that neither the selective pressure imposed by humans nor predatory behavior appear, on their own, to be responsible for the absence of functional organization in rodents. As outlined above, there are many additional differences between species that could account for the absence or presence of columns in visual cortex. We should also consider, however, that the capricious appearance of this organization may indicate that a deeper understanding of cortical computations and circuitry will not be achieved by identifying those conditions. Even if cortical columns were epiphenomenonal or have little computational advantage (Horton and Adams 2005), we will

gain insight into the fundamental structure of the neocortex by understanding their emergence.

## DISCLOSURES

No conflicts of interest, financial or otherwise, are declared by the authors.

## AUTHOR CONTRIBUTIONS

B.S. performed experiments; B.S., J.J.P., and N.J.P. analyzed data; B.S., J.J.P., and N.J.P. interpreted results of experiments; B.S. prepared figures; B.S. and J.J.P. drafted manuscript; B.S., J.J.P., A.R., and N.J.P. edited and revised manuscript; B.S., J.J.P., A.R., and N.J.P. approved final version of manuscript; N.J.P. conceived and designed research.

## REFERENCES

**Batschelet E.** *Circular Statistics in Biology*. London: Academic, 1981.

**Bonhoeffer T, Grinvald A.** Iso-orientation domains in cat visual cortex are arranged in pinwheel-like patterns. *Nature* 353: 429–431, 1991.

**Bosking WH, Zhang Y, Schofield B, Fitzpatrick D.** Orientation selectivity and the arrangement of horizontal connections in tree shrew striate cortex. *J Neurosci* 17: 2112–2127, 1997.

**Brainard D.** The Psychophysics Toolbox. *Spat Vis* 10: 433–436, 1997

**Carandini M, Ferster D.** Membrane potential and firing rate in cat primary visual cortex. *J Neurosci* 20: 470–484, 2000.

**Chapman B, Stryker MP, Bonhoeffer T.** Development of orientation preference maps in ferret primary visual cortex. *J Neurosci* 16: 6443–6453, 1996.

**Cheong SK, Tailby C, Solomon SG, Martin PR.** Cortical-like receptive fields in the lateral geniculate nucleus of marmoset monkeys. *J Neurosci* 33: 6864–6876, 2013.

**Clark TA, Scholl B, Priebe NJ.** A high density region of retinal ganglion cells in the grasshopper mouse. Program No. 447.08. 2014 Neuroscience Meeting Planner. Washington, DC: Society for Neuroscience, 2014. Online.

**Cleland BG, Levick WR.** Properties of rarely encountered types of ganglion cells in the cat's retina and an overall classification. *J Physiol* 240: 457–492, 1974.

**Dacey DM.** Physiology, morphology and spatial densities of identified ganglion cell types in primate retina. *Ciba Found Symp* 184: 12–28, 1994.

**Daniels JD, Norman JL, Pettigrew JD.** Biases for oriented moving bars in lateral geniculate nucleus neurons of normal and stripe-reared cats. *Exp Brain Res* 29: 155–172, 1977.

**DeFelipe J.** The evolution of the brain, the human nature of cortical circuits, and intellectual creativity. *Front Neuroanat* 5: 29, 2011.

**de Nó RL.** Cerebral cortex: architecture, intracortical connections, motor projections. In: *Physiology of the Nervous System*. Oxford: Oxford Univ. Press, 1949, p. 288–330.

**Dräger UC.** Receptive fields of single cells and topography in mouse visual cortex. *J Comp Neurol* 160: 269–290, 1975.

**Essen DC, Zeki SM.** The topographic organization of rhesus monkey prestriate cortex. *J Physiol* 277: 193–226, 1978.

**Garaschuk O, Milos RI, Konnerth A.** Targeted bulk-loading of fluorescent indicators for two-photon brain imaging in vivo. *Nat Protoc* 1: 380–386, 2006.

**Golshani P, Portera-Cailliau C.** In vivo 2-photon calcium imaging in layer 2/3 of mice. *J Vis Exp* 13: 681, 2008.

**Grienberger C, Konnerth A.** Imaging Calcium in Neurons. *Neuron* 73: 862–885, 2012.

**Horner BE, Taylor JM, Padykula HA.** Food habits and gastric morphology of the grasshopper mouse. *J Mammal* 25: 513–535, 1964.

**Horton JC, Adams DL.** The cortical column: a structure without a function. *Philos Trans R Soc Lond B Biol Sci* 360: 837–862, 2005.

**Hubel DH, Wiesel TN.** Receptive fields, binocular interaction and functional architecture in the cat's visual cortex. *J Physiol* 160: 106–154, 1962.

**Hubel DH, Wiesel TN.** Shape and arrangement of columns in cat's striate cortex. *J Physiol* 165: 559–568, 1963.

**Hubel DH, Wiesel TN.** Receptive fields and functional architecture of monkey striate cortex. *J Physiol* 195: 215–243, 1968.

**Hughes A.** Topographical relationships between the anatomy and physiology of the rabbit visual system. *Doc Ophthalmol* 30: 33–159, 1971.

**Jeon CJ, Strettoi E, Masland RH.** The major cell populations of the mouse retina. *J Neurosci* 18: 8936–8946, 1998.

**Kaschube M, Schnabel M, Löwel S, Coppola DM, White LE, Wolf F.** Universality in the evolution of orientation columns in the visual cortex. *Science* 330: 1113–1116, 2010.

**Keil W, Kaschube M, Schnabel M, Kisvarday ZF.** Response to Comment on "Universality in the evolution of orientation columns in the visual cortex". *Science* 336: 413, 2012.

**Kerr J, Greenberg D, Helmchen F.** Imaging input and output of neocortical networks in vivo. *Proc Natl Acad Sci USA* 102: 14063–14068, 2005.

**Landry SO.** The rodentia as omnivores. *Q Rev Biol* 45: 351–372, 1970.

**Langley WM.** Comparison of predatory behaviors of deer mice (*Peromyscus maniculatus*) and grasshopper mice (*Onychomys leucogaster*). *J Comp Psychol* 108: 394–400, 1994.

**Lee BB, Creutzfeldt OD, Elepfandt A.** The responses of magno- and parvocellular cells of the monkey's lateral geniculate body to moving stimuli. *Exp Brain Res* 35: 547–557, 1979.

**Levick WR, Thibos LN.** Analysis of orientation bias in cat retina. *J Physiol* 329: 243–261, 1982.

**Marshel JH, Kaye AP, Nauhaus I, Callaway EM.** Anterior-posterior direction opponency in the superficial mouse lateral geniculate nucleus. *Neuron* 76: 713–720, 2012.

**McLoughlin N, Schiessl I.** Orientation selectivity in the common marmoset (*Callithrix jacchus*): the periodicity of orientation columns in V1 and V2. *Neuroimage* 31: 76–85, 2006.

**Métin C, Godement P, Imbert M.** The primary visual cortex in the mouse: receptive field properties and functional organization. *Exp Brain Res* 69: 594–612, 1988.

**Mountcastle VB.** Modality and topographic properties of single neurons of cat's somatic sensory cortex. *J Neurophysiol* 20: 408–434, 1957.

**Murphy EH, Berman N.** The rabbit and the cat: a comparison of some features of response properties of single cells in the primary visual cortex. *J Comp Neurol* 188: 401–427, 1979.

**Nauhaus I, Nielsen KJ, Callaway EM.** Nonlinearity of two-photon $Ca^{2+}$ imaging yields distorted measurements of tuning for V1 neuronal populations. *J Neurophysiol* 107: 923–936, 2012a.

**Nauhaus I, Nielsen KJ, Disney AA, Callaway EM.** Orthogonal microorganization of orientation and spatial frequency in primate primary visual cortex. *Nat Neurosci* 15: 1683–1690, 2012b.

**Niell CM, Stryker MP.** Highly selective receptive fields in mouse visual cortex. *J Neurosci* 28: 7520–7536, 2008.

**Ogden TE.** The receptor mosaic of *Aotes trivirgatus*: distribution of rods and cones. *J Comp Neurol* 163: 193–202, 1975.

**Ohki K, Reid RC.** Specificity and randomness in the visual cortex. *Curr Opin Neurobiol* 17: 401–407, 2007.

**Ohki K, Chung S, Ch'ng Y, Kara P, Reid RC.** Functional imaging with cellular resolution reveals precise micro-architecture in visual cortex. *Nature* 433: 597–603, 2005.

**O'Keefe LP, Levitt JB, Kiper DC, Shapley RM, Movshon JA.** Functional organization of owl monkey lateral geniculate nucleus and visual cortex. *J Neurophysiol* 80: 594–609, 1998.

**Passaglia CL, Troy JB, Rüttiger L, Lee BB.** Orientation sensitivity of ganglion cells in primate retina. *Vision Res* 42: 683–694, 2002.

**Pelli D.** The VideoToolbox software for visual psychophysics: transforming numbers into movies. *Spat Vis* 10: 437–442, 1997.

**Piscopo DM, El-Danaf RN, Huberman AD, Niell CM.** Diverse visual features encoded in mouse lateral geniculate nucleus. *J Neurosci* 33: 4642–4656, 2013.

**Rakic P.** Evolution of the neocortex: a perspective from developmental biology. *Nat Rev Neurosci* 10: 724–735, 2009.

**Ramachandran VS, Clarke PGH, Whitteridge D.** Cells selective to binocular disparity in the cortex of newborn lambs. *Nature* 268: 333–335, 1977.

**Ringach DL, Mineault PJ, Tring E, Olivas ND, Garcia-Junco-Clemente P, Trachtenberg JT.** Spatial clustering of tuning in mouse primary visual cortex. *Nat Commun* 7: 12270, 2016.

**Ringach DL, Shapley RM, Hawken MJ.** Orientation selectivity in macaque V1: diversity and laminar dependence. *J Neurosci* 22: 5639–5651, 2002.

**Rowe AH, Rowe MP.** Physiological resistance of grasshopper mice (*Onychomys* spp.) to Arizona bark scorpion (*Centruroides exilicauda*) venom. *Toxicon* 52: 597–605, 2008.

**Rowe AH, Xiao Y, Rowe MP, Cummins TR, Zakon HH.** Voltage-gated sodium channel in grasshopper mice defends against bark scorpion toxin. *Science* 342: 441–446, 2013.

**Ruffer DG.** Agonistic behavior of the northern grasshopper mouse (*Onychomys leucogaster breviauritus*). *J Mammal* 49: 481–487, 1968.

**Sanes JR, Masland RH.** The types of retinal ganglion cells: current status and implications for neuronal classification. *Annu Rev Neurosci* 38: 221–246, 2015.

**Sarko DK, Leitch DB, Girard I, Sikes RS, Catania KC.** Organization of somatosensory cortex in the Northern grasshopper mouse (*Onychomys leucogaster*), a predatory rodent. *J Comp Neurol* 519: 64–74, 2011.

**Sarnaik R, Wang BS, Cang J.** Experience-dependent and independent binocular correspondence of receptive field subregions in mouse visual cortex. *Cereb Cortex* 24: 1658–1670, 2014.

**Scholl B, Burge J, Priebe NJ.** Binocular integration and disparity selectivity in mouse primary visual cortex. *J Neurophysiol* 109: 3013–3024, 2013a.

**Scholl B, Pattadkal JJ, Dilly GA, Zemelman BV, Priebe NJ.** Local integration accounts for weak selectivity of mouse neocortical parvalbumin interneurons. *Neuron* 87: 424–436, 2015.

**Scholl B, Tan AY, Corey J, Priebe NJ.** Emergence of orientation selectivity in the Mammalian visual pathway. *J Neurosci* 33: 10616–10624, 2013b.

**Soodak RE, Shapley RM, Kaplan E.** Linear mechanism of orientation tuning in the retina and lateral geniculate nucleus of the cat. *J Neurophysiol* 58: 267–275, 1987.

**Stosiek C, Garaschuk O, Holthoff K, Konnerth A.** In vivo two-photon calcium imaging of neuronal networks. *Proc Natl Acad Sci USA* 100: 7319–7324, 2003.

**Tan AY, Brown BD, Scholl B, Mohanty D, Priebe NJ.** Orientation selectivity of synaptic input to neurons in mouse and cat primary visual cortex. *J Neurosci* 31: 12339–12350, 2011.

**Timberlake W, Washburne DL.** Feeding ecology and laboratory predatory behavior toward live and artificial moving prey in seven rodent species. *Anim Learn Behav* 17: 1–10, 1989.

**Ts'o DY, Frostig RD, Lieke EE, Grinvald A.** Functional organization of primate visual cortex revealed by high resolution optical imaging. *Science* 249: 417–420, 1990.

**Van Hooser SD.** Similarity and diveristy in visual cortex: Is there a unifying theory of cortical computation? *Neuroscientist* 13: 639–656, 2007.

**Van Hooser SD, Heimel JAF, Chung S, Nelson SB, Toth LJ.** Orientation selectivity without orientation maps in visual cortex of a highly visual mammal. *J Neurosci* 25: 19–28, 2005.

**Vidyasagar TR, Urbas JV.** Orientation sensitivity of cat LGN neurones with and without inputs from visual cortical areas 17 and 18. *Exp Brain Res* 46: 157–169, 1982.

**Weliky M, Bosking WH, Fitzpatrick D.** A systematic map of direction preference in primary visual cortex. *Nature* 379: 725–728, 1996.

**Wikler KC, Rakic P.** Distribution of photoreceptor subtypes in the retina of diurnal and nocturnal primates. *J Neurosci* 10: 3390–3401, 1990.

**Xu X, Bosking W, Sáry G, Stefansic J, Shima D, Casagrande V.** Functional organization of visual cortex in the owl monkey. *J Neurosci* 24: 6237–6247, 2004.

**Xu X, Bosking WH, White LE, Fitzpatrick D, Casagrande VA.** Functional organization of visual cortex in the prosimian bush baby revealed by optical imaging of intrinsic signals. *J Neurophysiol* 94: 2748–2762, 2005.

**Xu X, Ichida J, Shostak Y, Bonds AB, Casagrande VA.** Are primate lateral geniculate nucleus (LGN) cells really sensitive to orientation or direction? *Vis Neurosci* 19: 97–108, 2002.

**Zaltsman JB, Heimel JA, Van Hooser SD.** Weak orientation and direction selectivity in lateral geniculate nucleus representing central vision in the gray squirrel *Sciurus carolinensis*. *J Neurophysiol* 113: 2987–2997, 2015.

**Zhao X, Chen H, Liu X, Cang J.** Orientation-selective responses in the mouse lateral geniculate nucleus. *J Neurosci* 33: 12751–12763, 2013.